Journal of Energy Chemistry 68 (2022) 255–266

Contents lists available at ScienceDirect

Journal of Energy Chemistry

journal homepage: www.elsevier.com/locate/jechem

http://www.journals.elsevier.com/journal-of-energy-chemistry/

A techno-economic and life cycle assessment for the production of green methanol from CO_2: catalyst and process bottlenecks

Tomas Cordero-Lanzac [a,1,2], Adrian Ramirez [b,1], Alberto Navajas [c,d], Lieven Gevers [b], Sirio Brunialti [e], Luis M. Gandía [c,d], Andrés T. Aguayo [a], S. Mani Sarathy [e], Jorge Gascon [b,*]

[a] Department of Chemical Engineering, University of the Basque Country (UPV/EHU), PO Box 644, 48080 Bilbao, Spain
[b] King Abdullah University of Science and Technology, KAUST Catalysis Center (KCC), Advanced Catalytic Materials, Thuwal 23955, Saudi Arabia
[c] Department of Science, Public University of Navarre (UPNA), Arrosadía Campus s/n, 31006 Pamplona, Spain
[d] Institute for Advanced Materials and Mathematics (InaMat^2), Universidad Pública de Navarra (UPNA), Edificio Jerónimo de Ayanz, Campus de Arrosadia, Pamplona-Iruña 31006, Spain
[e] King Abdullah University of Science and Technology, Clean Combustion Research Center (CCRC), Thuwal 23955, Saudi Arabia

ARTICLE INFO

Article history:
Received 22 August 2021
Revised 19 September 2021
Accepted 25 September 2021
Available online 26 October 2021

Keywords:
CO_2
Methanol
Kinetic modeling
Process simulation
Life cycle assessment

ABSTRACT

The success of catalytic schemes for the large-scale valorization of CO_2 does not only depend on the development of active, selective and stable catalytic materials but also on the overall process design. Here we present a multidisciplinary study (from catalyst to plant and techno-economic/lifecycle analysis) for the production of green methanol from renewable H_2 and CO_2. We combine an in-depth kinetic analysis of one of the most promising recently reported methanol-synthesis catalysts (InCo) with a thorough process simulation and techno-economic assessment. We then perform a life cycle assessment of the simulated process to gauge the real environmental impact of green methanol production from CO_2. Our results indicate that up to 1.75 ton of CO_2 can be abated per ton of produced methanol only if renewable energy is used to run the process, while the sensitivity analysis suggest that either rock-bottom H_2 prices (1.5 \$ kg^{-1}) or severe CO_2 taxation (300 \$ per ton) are needed for a profitable methanol plant. Besides, we herein highlight and analyze some critical bottlenecks of the process. Especial attention has been paid to the contribution of H_2 to the overall plant costs, CH_4 trace formation, and purity and costs of raw gases. In addition to providing important information for policy makers and industrialists, directions for catalyst (and therefore process) improvements are outlined.

1. Introduction

The high environmental impact of greenhouse gas emissions requires the development of technologies for the capture, storage and valorization of CO_2. In this scenario, the catalytic conversion of captured CO_2 has attracted a great deal of attention over the last few decades. Production of methanol, dimethyl ether and other hydrocarbons is amidst the most studied CO_2 hydrogenation processes [1,2]. Among these possibilities, methanol stands out [3,4], thanks to its versatility as commodity chemical, potential as a marine fuel, and as feedstock for the manufacture of intermediate chemicals and even more complex road transport fuels [5]. Not surprisingly, the large-scale production of green methanol is being sought after by both industry and academia.

Within the strategies for CO_2 valorization through catalytic technologies, insightful results have been reported for its electrochemical [6] and photochemical transformation [7]. In that sense, recent publications have reported the potential of electrofuels from CO_2. Brynolf et al. [8] reviewed the production cost estimates of this technology, which could potentially be competitive by 2030 according to the developments of technology. Regarding life cycle assessments (LCAs) of electrofuels, there is no doubt that greenhouse gas emissions can be clearly decreased by circa 90%, values that change depending on the considered boundary conditions [9]. Nevertheless, the uncertainty of calculations was also highlighted, as well as the high costs associated with these new technologies, mainly caused by electrolizer capital costs and stack life [8].

For these reasons, when considering the current technology readiness level (TRL) of these technologies, thermocatalytic pro-

* Corresponding author.
E-mail address: jorge.gascon@kaust.edu.sa (J. Gascon).
[1] These authors contributed equally to this work.
[2] Present address: Centre for Materials Science and Nanotechnology (SMN), Department of Chemistry, University of Oslo, N-0315 Oslo, Norway.

https://doi.org/10.1016/j.jechem.2021.09.045

cesses seem to be far ahead in terms of industrial implementation. In the field of thermocatalytic CO_2 hydrogenation to methanol, in addition to a large number of studies focusing on the classical syngas methanol synthesis catalyst, Cu-ZnO-Al_2O_3, several new systems have been recently reported, with ZnO-ZrO_2 [10], Pt-based [11] and In_2O_3/ZrO_2 catalysts being among the most promising solids in terms of methanol selectivity under mild reaction conditions [12,13]. Indium oxide has been reported as a highly active catalyst to produce methanol. The activation of CO_2 takes place over the active sites generated by In_2O_3 and an oxygen vacancy derived from the ZrO_2, and the stability of the catalyst depends on the In reducibility [13]. In a previous work, an In_2O_3/Co catalyst was presented as a promising alternative to the Zr-based catalyst [14]. Computational catalysis proved that the reaction is driven by the same mechanism, with oxygen vacancies being derived from Co. The obtained results in terms of methanol selectivity (>80%) and productivity (0.86 $g_{CH3OH}\ g^{-1}_{catalyst} h^{-1}$) at near thermodynamic equilibrium conversion place this new catalyst among the state of the art [14].

Catalyst development is, however, only one (although very important) hurdle to overcome when improving green methanol production; equally important is the overall process that determines the economic feasibility of the manufacture route. In order to gain insight into process performance, understanding (and modelling) reaction kinetics is a must. Vanden Bussche and Froment [15] proposed a steady-state kinetic model for the CO_2 hydrogenation to methanol considering all the individual steps involved in the process, including thermodynamic considerations. After simplifications, the system was described by apparent kinetic and adsorption constants. More recently, Seidel et al. [16] reported a comparison of a complex model with a Langmuir-Hinshelwood model, resulting in a very accurate estimation of experimental results in both cases. Indeed, Langmuir-Hinshelwood models have shown reliable overall fitting of experimental data for CO_2 hydrogenation using different catalysts and conditions [17–20].

Using similar kinetic models, albeit based on outdated data for the commercial Cu-ZnO-Al_2O_3 catalyst, several groups have carried out steady-state simulations of a methanol plant using Aspen Plus [21–24]. Most of these studies propose a similar plant outline, incorporating compression and separation stages and reactant recirculation along with the catalytic reactor. These simulations can be used to predict the amount of CO_2 abated by the production plant [21], estimate the viability of the process as a function of reactant price fluctuation [23], and calculate the carbon tax that would make the process economically viable [24]. However, as recently highlighted by Nestler et al. [19], in most cases these simulations have relied either on outdated Cu-ZnO-Al_2O_3 kinetic models or on models derived under conditions far from those of the actual plant operation. Moreover, these studies provide limited insights into the process bottlenecks. Indeed, CH_4 trace formation, the raw gas source (and therefore purity and cost), the influence of the energy source in the final CO_2 abatement, the impact of the different process costs (i.e., CAPEX, raw materials, utilities) on the breakeven MeOH price, or the maximum O_2 content in the system (which can alter the catalyst performance, especially for the Cu-ZnO-Al_2O_3 commercial system) have been largely overlooked in the open literature.

Hence, in order to address the issues highlighted above, we present a full multidisciplinary approach that should give the most updated economic analysis on green methanol synthesis. We first describe the catalyst material and perform the corresponding kinetic fitting. This is followed by detailed process modeling using the developed realistic kinetics. We then study how process variables impact the techno-economics of green methanol production. Lastly, we perform a life cycle assessment of the process to assess the real environmental impact and determine the main process bottlenecks.

2. Materials and methods

2.1. Chemicals

Cobalt acetate ($Co(CH_3COO)_2{\cdot}6H_2O$, Aldrich), indium acetate ($In(CH_3COO)_3{\cdot}xH_2O$, Aldrich), hydrogen peroxide (H_2O_2, 23% solution in water, Aldrich) and ammonia hydroxide (NH_4OH, Aldrich) were used as received. The commercial Cu-ZnO-Al_2O_3 catalyst was purchased from Alfa-Aesar.

2.2. Catalyst preparation

The catalyst was prepared via co-precipitation method following the procedure detailed elsewhere [14]. Briefly, 3.49 g of $Co(CH_3COO)_2{\cdot}6H_2O$ and 1.02 g of $In(CH_3COO)_3$ were dissolved in 35 mL of H_2O. Separately, 1.39 mg of H_2O_2 and 35 mL of 28% ammonia hydroxide solution were diluted with H_2O to 315 mL. Then, the salts-containing solution was added dropwise to the stirred ammonia hydroxide solution with a flow rate of 2 mL min^{-1}. The formed powder, denoted as InCo, was recovered and washed via centrifuging and subsequently dried at 60 °C. The washing protocol was repeated for three times.

2.3. Catalytic tests

Catalytic tests were carried out in a 16 channel Flowrence® from Avantium. Samples of the InCo catalyst were loaded in 15 of the channels, using the remaining one as a blank without catalyst. Prior to the reactions, the tubes were pressurized to 50 bar using a membrane-based pressure controller and the temperature was set to 300 °C. After 24 h of pretreatment under the reaction flows, experimental runs were carried out in the pressure range of 30–50 bar at 250–350 °C, using space time values up to 11 g h mol^{-1}_{CO2}, a total flow of 13 cm^3 (STD) min^{-1} per channel, and H_2/CO_2 molar ratios of 3–4. A small constant concentration of He was mixed with the feed as internal standard.

The reaction products were analyzed online using an Agilent 7890B GC with two sample loops. One sample loop goes to a TCD channel with 2 Haysep pre-column and MS5A, where He, H_2, CH_4 and CO are separated. Gases that have longer retention times than CO_2 on the Haysep column (Column 4 Haysep Q 0.5m G3591-80023) are back-flushed. Further separation of permanent gases is done on another Haysep column (Column 5 Haysep Q 6 Ft G3591-80013) to separate CO_2 before going to MS5A. The second sample loop goes to a FID with an Innowax pre-column (5 m, 0.20 mm OD, 0.4 μm film), a Gaspro column (Gaspro 30 M, 0.32 mm OD) and another Innowax column (45 m, 0.2 mm OD, 0.4 μm). Gaspro column separates C_1–C_8, paraffins and olefins. Innowax separates oxygenates and aromatics.

The CO_2 conversion (X_{CO_2}, %) and selectivity of each i product (S_i, %) in terms of contained C units are defined as follows:

$$X_{CO_2} = \left(1 - \frac{C_{He,blk} C_{CO_2,R}}{C_{He,R} C_{CO_2,blk}}\right) 100, \quad (1)$$

$$S_i = \frac{\frac{n_i C_{i,R}}{C_{He,R}}}{\frac{C_{CO_2,blk}}{C_{He,blk}} - \frac{C_{CO_2,R}}{C_{He,R}}} 100, \quad (2)$$

where $C_{He,blk}$, $C_{He,R}$, $C_{CO_2,blk}$, $C_{CO_2,R}$ are the concentrations of He in the blank, He in the reactor effluent, CO_2 in the blank, and CO_2 in the reactor effluent, respectively, and $C_{i,R}$ is the concentration of each i product in the reactor effluent with n_i carbon atoms. The carbon balance closure was higher than 97.5% in all cases. Each experiment was repeated four times, and the composition was computed by

average values of the results. Please note that negligible conversion of CO_2 to MeOH, CO or CH_4 was observed in all blank tests.

2.4. Kinetic modeling methodology

The kinetic model for the conversion of CO_2 into methanol was developed using the convection–dispersion-reaction equation, accounting for the mass conservation equation of each component of the reaction medium. Several simplifications can be assumed due to the characteristics of the system. The catalytic tests were performed during 180 h in a sequence that includes repeated control experiments. Deactivation was not observed, and the catalyst activity remained constant during the duration of the experiments. This avoids the need for a time-dependent expression of the equation and the intrinsic kinetic model can be extracted from these steady-state experiments. Moreover, the reactor inner diameter is 2 mm, which completely avoids radial dispersion and permits modeling the flow as purely convective transport. Axial dispersion is assumed negligible due to the high enough gas flows in the small-diameter reactor, with Re up to 10^5. At these values, dispersion coefficient can be assumed as low as 0.2 $m^2\ s^{-1}$ [25], with Pe reactor number values of 10^2. The pressure in all channels was accurately controlled by a membrane system and temperature was maintained constant in each set of channels (temperature controllers for each group of 4 reactors). Therefore, isothermal and isobaric conditions can also be assumed. In summary, experimental runs were carried out at suitable conditions that allow the intrinsic kinetic parameters to be calculated using the steady-state design equation for a packed bed reactor. Then, for the molar fraction of each i component of the reaction medium,

$$\frac{F}{S}\frac{dy_i}{dl} = \rho r_i \tag{3}$$

is defined for a catalytic bed length within $0 < l < L$, where F is the molar flow rate, S is the reactor section, ρ is the catalytic bed density and r_i is the formation rate of each i compound. Although the contribution of axial dispersion is low, a negligible diffusion term was also used aiming at the stabilization of the mathematical method, as we explained elsewhere [26]. For that reason, the above mentioned Pe number was considered.

These formation rates are calculated from the reaction rate of each j step of the reaction network, described by the reverse water gas-shift reaction, the production of methanol from CO_2 and CO and the undesirable formation of methane (heavier hydrocarbons are not observed in the product stream),

$$CO_2 + H_2 \overset{1}{\leftrightarrows} CO + H_2O, \tag{4}$$

$$CO_2 + 3H_2 \overset{2}{\leftrightarrows} CH_3OH + H_2O, \tag{5}$$

$$CO + 2H_2 \overset{3}{\leftrightarrows} CH_3OH, \tag{6}$$

$$CO + 3H_2 \overset{4}{\rightarrow} CH_4 + H_2O. \tag{7}$$

The kinetic equations follow Langmuir-Hinshelwood expressions, defined as

$$r_1 = \frac{k_1\left(P_{CO_2}P_{H_2} - \frac{P_{CO}P_{H_2O}}{K_1}\right)}{1 + K_{CO_2}P_{CO_2} + K_{H_2O}P_{H_2O}}, \tag{8}$$

$$r_2 = \frac{k_2\left(P_{CO_2}P_{H_2}^3 - \frac{P_{CH_3OH}P_{H_2O}}{K_2}\right)}{1 + K_{CO_2}P_{CO_2} + K_{H_2O}P_{H_2O}}, \tag{9}$$

$$r_3 = \frac{k_3\left(P_{CO}P_{H_2}^2 - \frac{P_{CH_3OH}}{K_3}\right)}{1 + K_{CO_2}P_{CO_2} + K_{H_2O}P_{H_2O}}, \tag{10}$$

$$r_4 = \frac{k_4P_{CO}P_{H_2}^3}{1 + K_{CO_2}P_{CO_2} + K_{H_2O}P_{H_2O}} \tag{11}$$

with kinetic constants (k_j) being defined by a reparametrized form of the Arrhenius equation:

$$k_j = k_j^*\exp\left[-\frac{E_j}{R}\left(\frac{1}{T} - \frac{1}{T^*}\right)\right], \tag{12}$$

where k_j^* is the kinetic constant at the reference temperature T^*, E_j is the activation energy and R is the universal gas constant. The equilibrium constants (K_j) are estimated as a function of the temperature using the empirical correlations reported elsewhere [27]. The adsorption constants for the CO_2 and water (K_{CO_2} and K_{H_2O}, respectively) follow the van't Hoff equation:

$$K = K^*\exp\left[\frac{\Delta H}{R}\left(\frac{1}{T^*} - \frac{1}{T}\right)\right], \tag{13}$$

where K^* is the adsorption constant at the reference temperature T^* and ΔH is the enthalpy of adsorption. Note that, despite methanol adsorption could also limit reaction rates, it was not considered in the model because a significant improvement of experimental data was not observed probably due to its lower partial pressure in the reaction medium.

The system is solved using a Runge-Kutta method of orders 1–5, with k_j^*, E_j, K^* and ΔH being the parameters to be optimized. With this aim, an objective function based on the sum of square errors (SSE) between the calculated and experimental values of molar fractions (y_i and y_i^e, respectively) is defined as

$$SSE = \sum_{i=1}^{n_c}\omega_i\sum_{n=1}^{n_e}\left(y_i - y_i^e\right)_n^2, \tag{14}$$

where ω_i is the weight factor of each i compound and n_c and n_e are the number of compounds and experiments, respectively

2.5. Process simulation

Process simulations were carried out with steady-state simulation models developed in Aspen Plus® V8.8 software. The selected property method was SR-POLAR, based on an equation-of-state model by Schwarzentruber and Renon, which is an extension of the Redlich-Kwong-Soave equation of state. The Wegstein method was used for flowsheet convergence with a mass balance closure of the system was better than 99.99%. In line with the standard conventional plants, the annual productivity target of the system is 275 kton $year^{-1}$ of 99.5% purity MeOH. Economic analysis was carried out with the Economics Solver extension of Aspen Plus. The electricity price was set to 0.0775 k$ kWh^{-1}. For the CO_2 emissions associated with the electricity and steam utilities, natural gas was selected as fuel source with a CO_2 emission data source from US-EPA-RULE-E9-5711 (5.59 10^{-5} kg CO_2 per kJ). CO_2 emissions using these estimates were only considered for the conventional energy sources scenario. The CO_2 abated was then calculated as the total CO_2 reacted in the plant minus the CO_2 emitted by the process utilities following the above CO_2 emission data source.

The techno-economic assessment of a plant using the conventional Cu-ZnO-Al_2O_3 methanol catalyst was also carried out as a comparison scenario. In particular, the plant proposed by Szima et al. [28] was scaled in order to match the target output of 275 kton $year^{-1}$ of 99.5% purity MeOH. It should be noted that the com-

parison scenario was performed without accounting for detailed kinetics of the Cu-ZnO-Al_2O_3 catalyst.

2.6. Life cycle assessment

The LCA simulation of the methanol plant was carried out using the software GaBi® Pro. 9.5 together with the databases associated to this program. Processes located in the European Union were considered. Two study cases were evaluated: the first study case considers all energy supplies for the reaction and electrolysis to be provided by a mix of renewable sources (47% photovoltaic, 30% wind energy, and 27% hydraulic [29,30]) and thermal energy supplied by the combustion of hydrogen from water electrolysis (hydrogen combustion has been selected as the best way in terms of environmental impact for thermal energy production [31]); the second study case considers thermal energy to be supplied by the combustion of natural gas, electricity from a current standard mix and hydrogen from natural gas steam cracking. A cement plant was considered the source of CO_2 with amine based capture located next to the MeOH plant. In case 1, the H_2 electrolyzer was also considered to be close to the MeOH plant. Both cases were evaluated using the environmental indicators recommended by The European Platform on Life Cycle Assessment [32]. Detailed information on these indicators and the assumptions of each study cases can be found in the Supplementary Material.

3. Results and discussion

3.1. Experimental data fitting and kinetic modeling

Experimental runs were carried out across a wide range of reaction conditions to gather information on the effect of the main variables for the development of the kinetic model. Fig. 1 shows the evolution with temperature of the selectivity to products (methanol, CO, methane and hydrocarbons) and CO_2 conversion at 50 bar, H_2/CO_2 molar ratio of 4 and using different space time values of 3.7, 7.3 and 11.0 g h mol_{CO2}^{-1} (Fig. 1a–c, respectively). Each run was repeated at least three times, with the corresponding error bars being displayed in the conversion symbols; the reproducibility of the results is shown to be high. From the experimental points depicted in Fig. 1, we can observe that CO_2 conversion increases with temperature and space time and reaches a maximum value of ca. 25% at the extreme study case (350 °C and 11.0 g h mol_{CO2}^{-1}). Nevertheless, the product distribution is drastically modified as the reaction conditions are varied. Without considering the reaction at 250 °C and 3.7 g h mol_{CO2}^{-1}, which shows negligible conversion values, methanol selectivity significantly declines as temperature increases. This presumably occurs due to the disfavored equilibrium reaction of CO_2 conversion at higher temperatures [18]. Consequently, the selectivity to CO is increased with temperature. The concentration of CH_4 is also higher at 325 and 350 °C, which could be related to the promoted methanation reaction over the Co catalyst. A similar trend is observed with space time. The increase in the amount of catalyst leads to a higher extent of reaction, which decreases the selectivity to methanol and increases that of CO.

Aiming for maximum production of methanol in the simulated process, a compromise between conversion and selectivity must be reached. The evolution of methanol productivity in each of these experimental runs is depicted in Fig. S1. In all cases, a maximum of productivity is observed, which is displaced towards lower temperatures upon increasing the space time value. The overall maximum methanol production exhibited by the InCo catalyst (0.42 g $g^{-1}h^{-1}$) is located at the central experimental data point, at 50 bar, H_2/CO_2 molar ratio of 4, 300 °C and 7.3 g h $molCO_2^{-1}$. Note that runs at different pressures and H_2/CO_2 molar ratios were also used for the kinetic model computation, but methanol productivity was lower in all cases.

The kinetic modeling methodology (see Methods and Supplementary Material) and the collected experimental data were used in order to calculate the kinetic parameters that describe the catalytic system. The best fitting of the experimental data is obtained with the parameters listed in Table 1. The 95% confidence intervals, also shown in Table 1, were calculated from the discrepancies between experimental and calculated data. The value of the SSE obtained is ca. 0.04 and the standard deviation is ca. 0.02, which gives a very narrow normality plot for the kinetic parameter computation.

With the computed kinetic parameters, the initial reaction rates for CO and MeOH formation are estimated to be 5.1 10^{-3} and 1.7 10^{-2} mol $g^{-1}h^{-1}$, respectively. This is in agreement with most of the reported mechanistic studies, which suggest the prevalence of the direct mechanism of CO_2 to MeOH via formate and methoxy intermediates [33]. The order of magnitude of the computed constants is similar to that reported for a similar catalytic system with CO_2 conversions higher than 15% [34]. In terms of energy requirements, the values of apparent activation energy calculated for all the steps of the reaction network are within the 47–65 kJ mol^{-1} range, characteristic values of the kinetic regime. Especially, the value of the activation energy for the direct hydrogenation of CO_2 to methanol is within the range of those previously proposed by other authors with similar catalytic systems [18]. At our experimental conditions, the apparent activation energy for the rWGS reaction is slightly lower than that of methanol formation, which can also be explained by equilibrium-limited reaction at the integral regime used in this work. The adsorption heats for CO_2 and water are, as expected for an exothermic process, negative in value. The suitable fitting of the experimental data is more easily observed in Fig. 1(d–g), where the evolution with space time of the molar fractions of C-containing products is illustrated. The model predicts well the CO_2 conversion into CO and methanol. Moreover, the maximum concentrations of methanol previously observed at 300 and 325 °C are also estimated by the model. Experimental data fitting for reactions with lower H_2/CO_2 ratio and lower pressure is also shown in Fig. S2.

Although Fig. 1(d–g) show the evolution of C-containing products, the model also accounts for the consumption of H_2 and formation of water. Indeed, the partial pressures of both components play a key role in the reaction network (see Equations (8)–(11) and experimental data fitting in Figs. S3–S6). As expected, the concentration of H_2 decreases along with that of CO_2 and water is produced as a function of the conversion. Then, the higher the extent of the reaction, the more water is produced through the reverse water-gas shift reaction (Equation (4)) and the direct formation of methanol (Equation (5)). Management of these two carbon-free compounds is of a paramount importance for the process, as H_2 should be recirculated and H_2O should be condensed in order to maximize methanol production. Likewise, although its concentration is the lowest one at most conditions, the production of methane increases with space time, temperature, total pressure and H_2/CO_2 ratio. At this point, this experimental observation (well predicted by the model) should be considered for the simulation of the plant since recirculation and scaling-up will lead to an accumulation of this undesirable byproduct in the system, ultimately causing a pronounced decrease in methanol productivity. At the optimal conditions that will be simulated in the plant, the net formation rates of CO, methanol and methane are compared in Fig. S7. Despite the rates of methanol and CO formation being considerably higher (0.75 times lower that of CO at this temperature), methane is present in the product stream, with its formation rate being 0.14 times lower than that of methanol.

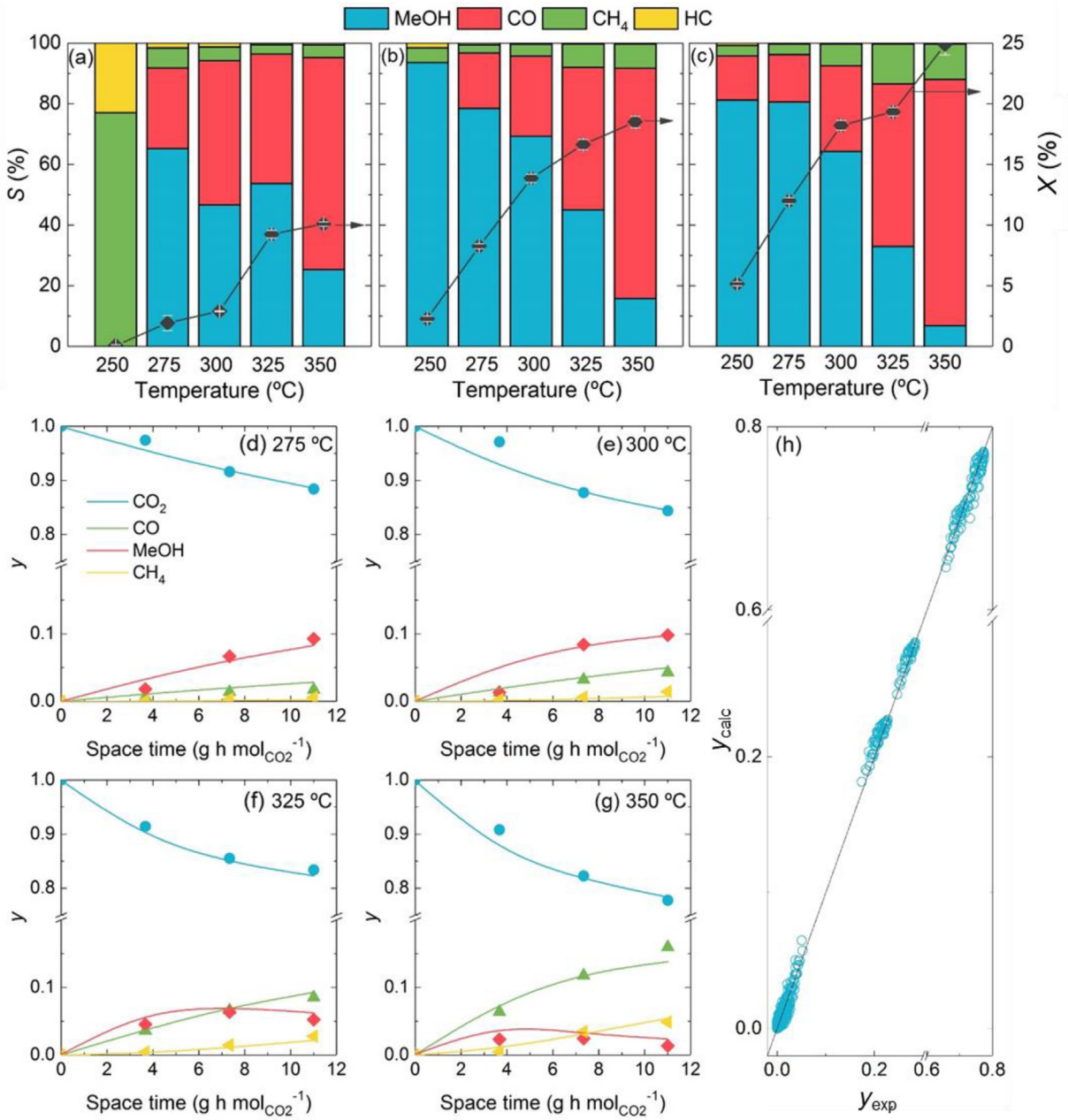

Fig 1. Evolution with temperature of the CO_2 conversion and products selectivity at 50 bar, H_2/CO_2 = 4 and using space time values of (a) 3.7, (b) 7.3 and (c) 11.0 g h mol_{CO2}^{-1}; comparison of the experimental data (symbols) with those estimated by the model (line) for the evolution with space time of the molar fractions at (d) 275, (e) 300, (f) 325 and (g) 350 °C. P = 50 bar, H_2/CO_2 = 4; (h) parity plot of the calculated and experimental molar fractions.

Table 1
Kinetic and adsorption constants at the reference temperature (300 °C), apparent activation energies and adsorption heats for the InCo intrinsic kinetic model.

	k^*, K^*	E, ΔH (kJ mol^{-1})
k_1 (mol $g^{-1}h^{-1}$ bar^{-2})	(1.38 ± 0.29) 10^{-4}	48.3 ± 2.7
k_2 (mol $g^{-1}h^{-1}$ bar^{-4})	(2.98 ± 0.53) 10^{-7}	52.9 ± 3.7
k_3 (mol $g^{-1}h^{-1}$ bar^{-3})	(5.70 ± 0.62) 10^{-6}	64.4 ± 2.7
k_4 (mol $g^{-1}h^{-1}$ bar^{-4})	(5.40 ± 0.59) 10^{-7}	47.7 ± 3.0
K_{CO2} (bar^{-1})	(9.79 ± 0.32) 10^{-1}	−6.3 ± 1.5
K_{H2O} (bar^{-1})	(1.36 ± 0.30) 10^{0}	−5.9 ± 1.0

As an overall fitting result, the parity plot in Fig. 1(h) shows the comparison of the experimental and calculated data for the 90 non-repeated runs fitted for the kinetic computation (from which the 95% confidence interval was estimated). Most of the dots are located at the diagonal and only few outliers are identified, validating the model.

3.2. Aspen Plus® process simulation

In our process simulation we targeted an annual productivity of 275 kton $year^{-1}$ of 99.5% purity MeOH, in line with standard conventional plants [35]. A simplification of the plant is illustrated in Fig. 2(a), whereas the detailed process model flowsheet is summarized in Fig. 2(b) and contains three main parts: the feeding stage, the reaction stage and the separation stage.

3.2.1. The feeding stage

To meet the desired product capacity, the process has a CO_2 feed of 1750 kmol h^{-1} and a H_2 feed of 5500 kmol, close to the 1:3 sto-

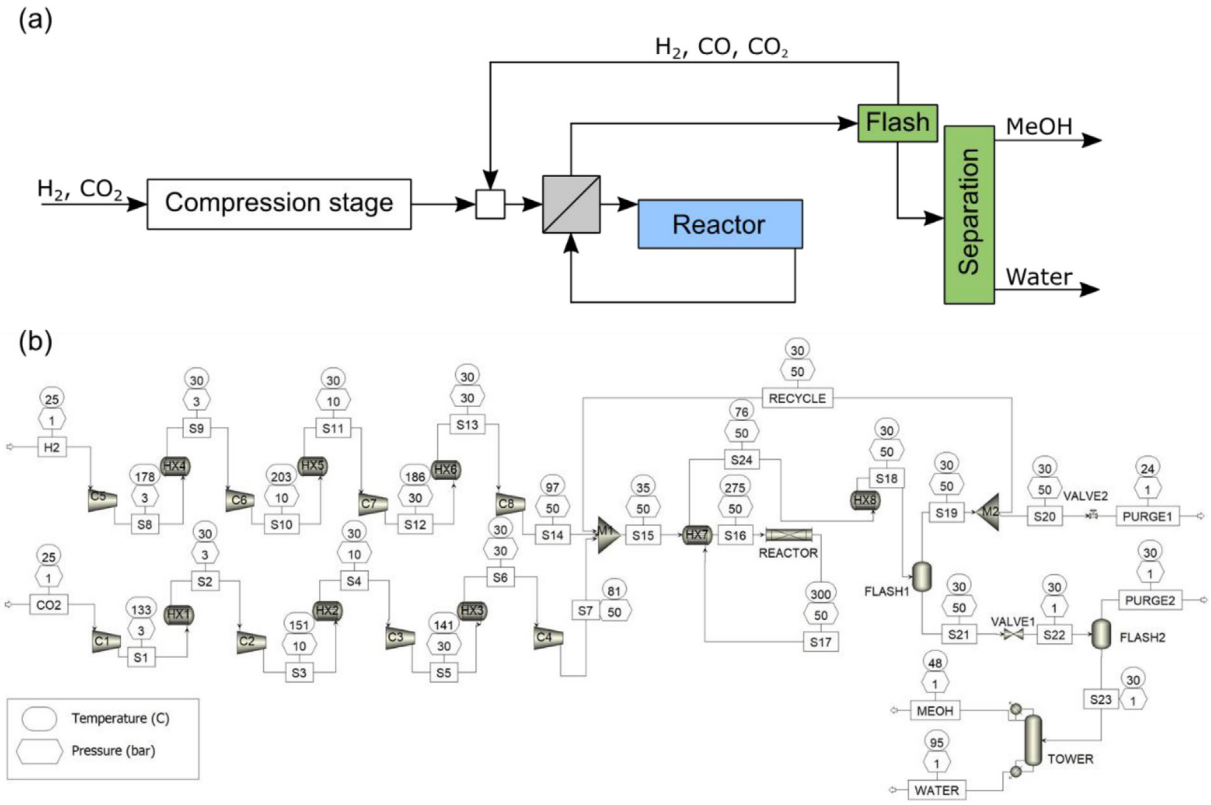

Fig 2. (a) Simplified scheme of the methanol plant (blue: reaction, green: separation, gray: heat integration) and (b) process flow diagram of the MeOH plant. Temperature and pressure values are presented for each stream.

ichiometric ratio. Both the CO_2 and H_2 feed are considered to be produced in external facilities. Taking the reactants recirculation into account, the CO_2-to-H_2 molar ratio in the reactor section is 1:4, as was previously observed to be the optimal one. The inlet conditions for both gases were assumed to be 1 bar and 25 °C. Both streams were compressed by 4 isentropic compressors (C1 to C4 for CO_2 and C5 to C8 for H_2) with intercooling heat exchangers (HX1 to HX6) to cool down the pressurized streams. The isentropic efficiency was set to 0.8 and the mechanical efficiencies to 0.95. Once pressurized at 50 bar, the streams were mixed (M1) together with the recycle stream.

3.2.2. The reaction stage

The pressurized mixed feed is first sent to a heat exchanger (HX7) to preheat the stream to 275 °C by using the heat of the product stream. The reactor is a Lurgi type tubular fixed bed reactor that operates at 300 °C and 50 bar. The number of tubes was 7500 with a length of 7.5 m and an internal diameter of 40 mm. The reactor is packed with 105 ton of InCo catalyst with a density of 2500 kg m^{-3} and a bed voidance of 0.5. The resulting space time and residence time of the gases are ca. 7.3 g h mol^{-1}_{CO2} (GHSV, 14,400 cm^3_{STP} h^{-1} g^{-1}) and 1.5 s, respectively. The kinetic model extracted from our experimental results was incorporated into the reactor simulation. The software required a specific input of the equation consisting in a kinetic factor, a driving force expression and an adsorption term along with SI units. The rearrangement of the kinetic parameters to the suitable form is detailed in the Supplementary Material. The reactor was tested isolated in order to validate the experimental results. The comparison of the experimental values, the satisfactory predictions of the intrinsic kinetic model for the InCo catalyst and those simulated for the reaction stage of our process are depicted in Fig. S8.

3.2.3. The separation stage

The reactor outlet at 300 °C and 50 bar is first cooled down to 30 °C in a heat exchanger (HX8). The cooled stream is then sent to a flash drum unit (Flash1) operating at 30 °C and 50 bar to remove the light gasses (CO, CH_4, and H_2). This gas stream is recycled back and mixed to the reactor feed with a 2.5% purge (Purge1). Based on our experimental observations and model predictions (Fig. 1), avoiding the production of methane is not completely possible at all conditions, which motivates the necessity of including this purge stream. The liquid stream is sent through a pressure relief valve to reduce the pressure to 1 bar and then to another flash drum (Flash2), operating at 25 °C and 1 bar to remove traces of CO_2 dissolved in water (Purge2). The liquid stream, rich in water and methanol, is sent to a RadFrac rigorous distillation column operating at 1 bar with 30 equilibrium stages final product purification. The condenser type is total condenser and the reboiler type is kettle. The reflux ratio is set to 2 and the final purity of the methanol stream is 99.5%.

3.3. Techno-economic evaluation (TEA)

The mass balance and composition of each stream of the process depicted in Fig. 2(b) can be found in Table S2. In total, 32.1 ton h^{-1} of methanol with a purity of 99.5% is produced in the plant. Assuming 8500 h $year^{-1}$ of operation, the plant will generate a total of 272,850 ton $year^{-1}$ of liquid methanol, close to the design value of the plant. The total thermal duty was −74 MW (34 MW of heating duty and 108 MW of cooling duty, mostly for cooling water) and total electrical power was 31.5 MW. The recycle of the light gases stream would allow an overall CO_2 conversion of 72.5% to be obtained in the process, almost 5 times higher than the experimental conversion per pass. Nevertheless, attempts to increase this conversion by reducing the purge ratio below 2.5%

were fruitless as CH_4 accumulated in the system to concentrations above 15%. Moreover, since the heating/cooling/compression steps are also an indirect source of CO_2 (see experimental section), the real CO_2 conversion (i.e., total CO_2 abated) decreases to 28.9% (purge ratio of 2.5%), with abated CO_2 quantities of 0.77 tons per ton of methanol produced (see Table 2). Hence, these numbers highlight the importance of using renewable energy to power up the plant as 55% of the CO_2 converted in the reactor will be offset if traditional fossil energy sources are used. In contrast, if only renewable energy sources are used and all these indirect sources of CO_2 are obviated, the CO_2 abated will jump to 1.75 tons per ton of methanol, a 225% increase.

To provide further insight, we estimated the size of the renewable energy source depending on its type and the associated CAPEX needed. As discussed above, the total electrical power is estimated in 32.5 MW. For solar photovoltaic cells (PV), on a capacity basis, the total-area capacity-weighted average is ca. 28 MW km^{-2} [36,37]. For typical average wind installation, this requirement is 5 MW km^{-2} [38]. Therefore, only considering the electricity, the methanol plant will require 1.16 km^2 of land if PV is used or 6.5 km^2 of land if wind is used. This later value can be further reduced by circa 40% if offshore wind farms are used due to their higher capacity density. Assuming now that CAPEX costs of PV and wind farms can be estimated in 500 and 1500 \$ kW^{-1}, respectively [39], the solar PV farm will cost ca. 16 M\$ and the wind farm will cost ca. 48 M\$. Both values are less than the methanol plant CAPEX. However, only approx. 40% of the CO_2 emissions of the plant come from the electricity used for the compressors (31.5 MW). The remaining 60% is due to the heating thermal duty (34.5 MW), meaning that virtually two times bigger PV or wind plants will be required, with a resulting CAPEX rivaling the one of the methanol plant alone. Hence, here we need to ponder that the integration of renewable energy comes with a huge associated cost that can double the initial CAPEX investing. Additionally, we also need to consider the intermittency of the renewable energy [40]. While the intermittency can be partially offset by combining different sources that complement each other (i.e., continental wind that tends to peak at night and solar that peaks with daylight), it might require external storage systems that can impact the initial investing. This could even lead to prohibitive MeOH costs above 1500 \$ ton^{-1} if intermittency is addressed solely by energy storage [41]. A much more reasonable approach is the flexible process with a variable load able to meet the annual target [41]. Hence, integration of renewable energy is not straightforward and individual studies for each particular plant capacity and/or location are necessary.

Following, the estimated equipment costs required for the operation are shown in Fig. 3(a). In addition, the values of individual costs can also be found in Table S3. As observed, two compressors account for more than 65% of the total equipment costs. Specifically, C5 and C6 compressors deal with H_2 compression from 1 bar to only 10 bar (please see the effect of final pressure on energy requirement for compression on Fig. S9). Hence, if green electrochemically generated hydrogen could be produced at least at 10 bar, the CAPEX would be reduced from 94 to 34 M\$. At this point, it is worth mentioning that most of the previous process simulation studies in the state of the art do not consider the H_2 compression [21–24], despite its obvious influence on CAPEX. Most of them only consider the simulation of the Cu-ZnO-Al_2O_3 commercial catalyst with the feed stream directly at 30 bars, thereby painting an unrealistic picture of the overall process. Only the work of Szima et al. [28] included the compression of reactants from atmospheric to 80 bar, which was also predicted as one of the most expensive operations of the process.

Next, we evaluated the economic viability of the proposed MeOH plant. For the initial analysis, the following material costs were used: 550 \$ ton_{MeOH}^{-1}, 50 \$ ton_{CO2}^{-1} and 3.5 \$ kg_{H2}^{-1}. The MeOH price was set based on the guidance provided by the Methanol Institute in their 2019 report on green methanol [42] and on the work of Bergins et al. from Mitsubishi Hitachi Power Systems [43]. A 20 year timeframe was considered for CAPEX amortization with a linear depreciation method. The results of overall costs are listed in Table 3 and depicted in Fig. 3(b). H_2 and CO_2 costs (325 M\$ $year^{-1}$) are two times the product sales (154 M\$ $year^{-1}$), making this process unfeasible. This high influence of the raw materials can be easily observed in Fig. 3(c), where the contribution of the different annualized process costs on the final MeOH price is evaluated. Up to 67.5% of the final MeOH price comes only from H_2, while CO_2 contributes to 16.5%. Similarly, the utilities account for 12.4% of the MeOH price of which almost 85% comes from the compression steps (see Fig. S10). Last, the CAPEX contribution to final MeOH price is only 2.2%. These numbers highlight the importance of including gas compression in the TEA and gives fair warning to the optimistic MeOH prices provided by current simulations in the state of the art. However, it could be reasonable to consider that grey and blue hydrogen can be produced and delivered at high pressure. This assumption should be avoided for green hydrogen produced in current electrolyzers, which work close to near atmospheric pressures, and therefore, this extra expense needs to be taken into consideration. In summary, the overall process can be considered low capital intensive, highly dependent on the raw material cost, and hindered by the energy costs required for H_2 compression.

Table 2
CO_2 mass balance for the MeOH process.

Variable	Value
Total CO_2 in (ton h^{-1})	77.0
Total CO_2 out (ton h^{-1})	22.2
Total CO_2 utilities (ton h^{-1})	30.2
Total CO_2 abated (ton h^{-1})	24.6
CO_2 abated (ton ton_{MeOH}^{-1})	0.77
Max CO_2 abated (ton ton_{MeOH}^{-1})[a]	1.75

[a] If only renewable energy sources are used, impact of the CO_2 source emissions is not included.

To better evaluate the raw materials effect on the net revenue (i.e., product sales-operating costs), a sensitivity analysis was performed focusing on H_2 and CO_2 (see Fig. 3d and e, respectively). As expected, the feasibility of the MeOH plant largely depends on H_2 and CO_2 prices. In particular, with the current MeOH plant design, the process would be economically viable with H_2 prices lower than 1.5 \$ kg^{-1} with a CO_2 price of 50 \$ ton^{-1}. Similarly, with the current H_2 price fixed at 3.5 \$ kg^{-1}, a taxation of CO_2 of at least 300 \$ ton^{-1} would be needed to obtain a positive revenue. The low price range of 1.5 \$ kg^{-1} is currently only feasible for blue/gray hydrogen from fossil fuels [44], while according to the recent Monte Carlo study of Yates et al. [45], the high range of 3.5 \$ kg^{-1} might not even be feasible for current PV electrolysis depending on the electrolyzer technology or location. To validate our simulations, TEA on the commercial Cu-ZnO-Al_2O_3 catalyst was also performed, scaling the model developed by Szima et al. [28] to match our system productivity target. Similar CAPEX, H_2 prices and CO_2 taxations are required to reach a MeOH breakeven of 550 \$ ton^{-1} (see section S7 in Supplementary Material), corroborating therefore our simulations and the high influence of the raw material costs.

3.4. Other process bottlenecks

An important factor that strongly affects the process that has not been considered up to now and is usually neglected in the lit-

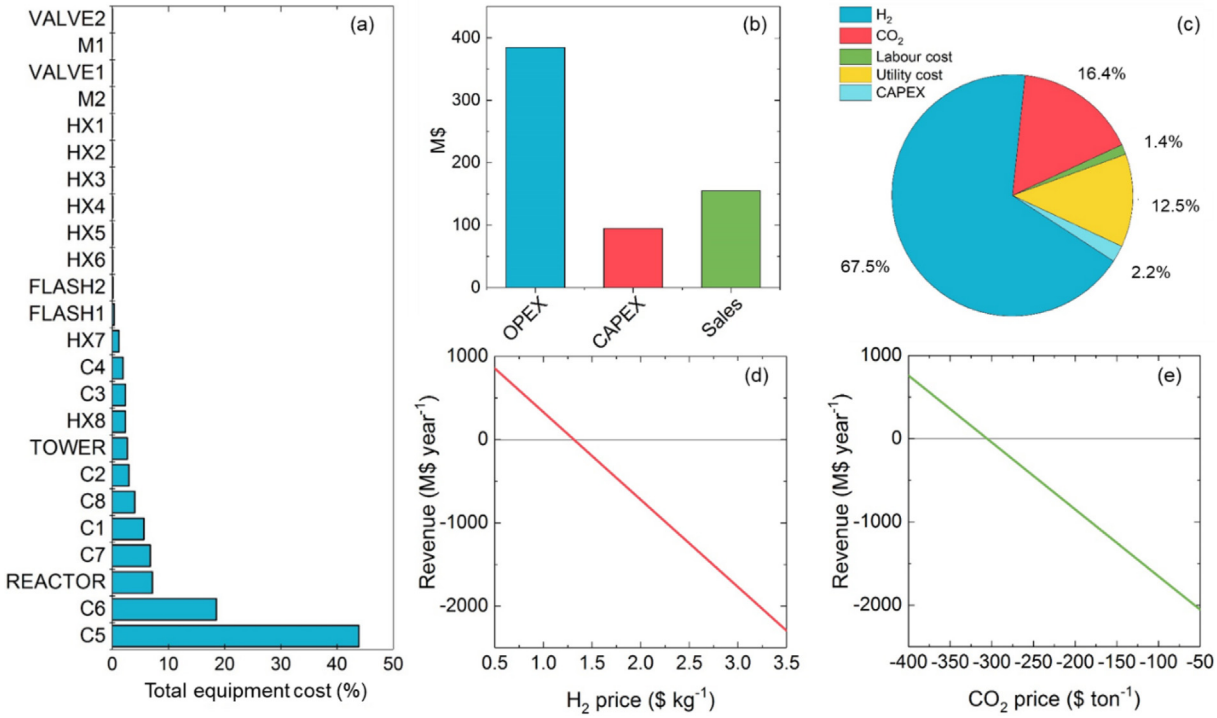

Fig 3. (a) Equipment cost distribution for the MeOH process; (b) overview of the main costs for the MeOH process. H_2 price fixed to 3.5 \$ kg^{-1} and CO_2 price to 50 \$ ton^{-1}; (c) contribution of the different annualized process costs on the final MeOH price (pattern in the utility pie represents the compression contribution); sensitivity analysis of the main raw materials cost: (d) H_2 price (CO_2 price fixed to 50 \$ ton^{-1}), (e) CO_2 cost (H_2 price fixed to 3.5 \$ kg^{-1}). MeOH price set to 550 \$ ton^{-1}.

Table 3
Summary of the cost evaluation for the MeOH process.

Variable	Value
Total capital cost (\$ ton^{-1}_{MeOH})	347.6
Equipment installed cost (\$ ton^{-1}_{MeOH})	209.6
Total operating cost (\$ ton^{-1}_{MeOH} $year^{-1}$)	1408.7
Raw materials cost (\$ ton^{-1}_{MeOH} $year^{-1}$)	1192.0
Utilities cost (\$ ton^{-1}_{MeOH} $year^{-1}$)	96.5
Total product sales (\$ ton^{-1}_{MeOH} $year^{-1}$)	567.9

erature is the inevitable formation of CH_4 during the process. Surprisingly, most of the reported kinetic models and process simulations for any of the MeOH catalysts on the state of the art do not take this constraint into account, modeling close to 100% recycle streams. Nonetheless, up to now, there is no reported catalyst able to totally suppress the formation of CH_4. By way of example, additional CO_2 hydrogenation reaction tests with the commercial Cu-ZnO-Al_2O_3 catalyst were conducted in a wide variety of conditions (see Table S4). Although low concentrations are achieved, the benchmark Cu-ZnO-Al_2O_3 catalyst produces CH_4 even under the most favorable reaction conditions. The InCo catalyst studied herein, which demonstrated a significant improvement of the process selectivity [14], also produces CH_4 (Fig. 1a–c). As a product whose separation is not considered in the plant, it must be taken into account in order to obtain realistic results of the operation.

First, the formation of CH_4 must be included as an individual step of the reaction network, which is commonly avoided aiming for computational simplifications. In this case, we performed experiments in a very wide range of temperatures, even higher than the optimal one. The goal was to obtain CH_4 concentrations in the effluent high enough to calculate kinetic parameters with mathematical significance. Then, when CH_4 is included in the catalytic system, it directly affects the design of the plant, because its accumulation limits the maximum recycle stream.

In order to illustrate this effect, additional simulations were performed for our InCo catalyst considering the real CH_4 production, half of the CH_4 production and no CH_4 production. For this, the kinetic constant of reaction (4) (Equation (11)) was adapted in each case. The resulting MeOH prices for the 3 cases as a function of the CO_2 and H_2 prices are depicted in Fig. S11. Indeed, the lower the CH_4 formation, the lower the MeOH final price can be, independently of the H_2 or CO_2 prices. For instance, with no CH_4 formation, MeOH prices close to the target of 550 \$ ton^{-1} can be achieved with a H_2 price of 2 \$ kg^{-1} (a very realistic approach) and without any CO_2 taxation. The reason behind this is the ability to increase the recycle stream by reducing the CH_4 formation, as its accumulation in the plant will be greatly suppressed. In our particular case, by reducing the CH_4 formation by half, we can increase the recycle from 97.5 to 99% without having a CH_4 accumulation above 15%. Consequently, the MeOH productivity of the process increases by 15%. In case of no CH_4 formation, the recycle stream can be further increased to 99.5%, thereby boosting MeOH productivity up to 30%.

Apart from CH_4, other undesired compounds can also affect the process in multiple ways rarely evaluated in most studies. For instance, the source of both CO_2 and H_2 will determine its purity and its price. Obviously, the highest purity means the highest production cost (see Table 4 [46]). This is especially important due to the already demonstrated high influence of the raw materials in the final MeOH cost (see Fig. 3c). Moreover, these traces can also affect the performance of the catalyst. As it has been reported, the commercial Cu-ZnO-Al_2O_3 cannot tolerate high concentrations of O_2 (300 ppm) or Cl (10 ppm) due to metal reoxidation and Cu metal poisoning (CuCl is formed), respectively [47]. To shed light on this hurdle, additional simulations were performed to investigate the accumulation of O_2 in the system when ppm of O_2 is fed with the reactants (see Fig. S12). Again, recirculation of gases (assumed at 99% for the simulations) leads to a magnification of the O_2 concentration in the system, especially when O_2 traces are con-

Table 4
Source, price and purity of the CO_2 feed [46].

Source	Price ($ ton^{-1})	CO_2 (%vol)	SO_x (ppm)	NO_x (ppm)	O_2 (ppm)	HCl (ppm)	H_2S (ppm)
Oxyfuel	82.68	77.69	127.31	446.3	76100	–	–
Oxyfuel	120.6	96.61	137.63	81	14000	–	–
Oxyfuel	135.26	99.99	138.69	20	5500	–	–
Post-combustion	118.95	99.99	102	10	–	349	–
Pre-combustion	25.32	97.64	–	–	–	–	3249

sidered in the H_2 feed stream. The 300 ppm limit established for the commercial Cu-ZnO-Al_2O_3 catalyst is obtained feeding only 145 ppm of O_2 in the H_2 stream. As the recycle stream increases, the process requires even lower O_2 concentrations in the feed stream, thereby increasing drastically the H_2 and CO_2 purity needed and hindering the positive recycle productivity. One possible solution could be to include a deoxygenation (deoxo) catalytic reactor [48] in the system after the first compression steps (see Fig. S13). The rationale of this location is to take advantage of the high temperature of the feed after compression (ca. 200 °C), enough to avoid any additional heat supply to the reactor, while still being below the 10 bar limit operation pressure of the deoxo process. However, these reactors cannot eliminate completely the O_2 in the system (ca. 10 ppm [49]), do not tolerate inlet O_2 concentrations higher than 0.8%, and are based on expensive Pt or Pd catalysts that need to be replaced every ca. 5 years [50], which will drastically increase the OPEX costs.

Summing up, although outstanding efforts have been made in recent years for the development of selective catalyst for methanol production from CO_2, the main process bottlenecks still need further investigation. Based on our results, a successful scale-up of the process will depend on non-catalytic variables as the reactant prices and their compression to the reaction pressure. Moreover, developing a catalyst that does not produce CH_4 or can withstand large oxygen impurities could have the greatest impact in the process. In particular, the absence of CH_4 could boost the productivity by minimizing the purges, whereas the increase in oxygen tolerance would allow low-cost feed gases to be used in the process, whose huge positive effects in the final MeOH breakeven price have been already discussed. For instance, in the particular case of green H_2 produced via water electrolysis, a great fraction of the costs comes from the oxygen removal after the electrolyzer [51,52]. Consequently, catalyst development, if done in the right direction, could avoid purification costs and greatly increase the viability of the plant.

3.5. Life cycle assessment

Due to the above discussed key contribution of reactants and the renewable energetic requirements to the process, a LCA of the MeOH plant was also carried out (see Methods and Supplementary Material). Diagrams for the two study cases are provided in Fig. 4(a) (renewable energy sources, case 1) and Fig. 4(b) (non-renewable sources, case 2). The functional unit of both cases studied is the production of 2.75 10^8 kg of methanol, which is the production of the plant along one year with 8500 h working per year. A summary of the TEA estimation for the two study cases is summarized in Table S5. Fig. 5(a) shows the comparison of both study cases, with the values of each indicator being summarized in Tables S7 and S8. As observed, 10 of the 16 evaluated indicators are lower in the study case 1, highlighting the global warming potential (GWP) indicator that is reduced from 1.7 to − 4.2 kg 10^8 CO_2 eq. when renewable energies are used to run the plant. Hence, in line with the above TEA discussion, we can resolve that it does not make sense to produce MeOH from CO_2 if all the energy requirements are also not renewable. Nevertheless, we also need to highlight that some indicators, specially the ozone depletion potential (ODP), land use (LU) and water use (WU) are higher in case 1.

The relative contribution of the process variables to each indicator in both study cases is detailed in Fig. 5(b and c), respectively. As expected, a significantly higher contribution of electricity production (yellow bars) from the non-renewable sources can be easily observed for the study case 2. We can also observe that the contribution of CO_2 capture is negative on the GWP due to its consumption in the process and that, in the second case, the emission related with the energy supply and hydrogen production via steam cracking can actually overcome the CO_2 consumption. Those indicators with higher values in the study case 1 are mainly associated with the renewable source requirements. H_2 is the main contributor to ODP, LU and WU indicators, which is explained by photovoltaic and hydraulic energy production. Some indicators as HTC (human toxicity potential, cancer effects) and RDM (resource use of minerals and metals) are mainly related to the catalyst production and are unavoidable. The CO_2 capture process via amines (green bars) also negatively impacts most of the indicators expect the GWP. Nevertheless, although the different distribution on each indicator, we can consider that, overall, H_2 production (red bars) is the most environmentally impactful variable of the process for both cases, as well as the most expensive resource as predicted by the TEA (Fig. 3).

Following, we have compared the MeOH price and the normalized GWP per ton of MeOH produced of our process with the ones obtained in the production of MeOH via conventional sources, i.e., natural gas and coal [53,54] (see Fig. 6). As expected, the MeOH prices that can be obtained from coal or natural gas are lower than the 550 $ ton^{-1}_{MeOH} target of the CO_2 valorization process (which is even hard to reach as the above TEA revealed). Nevertheless, when looking at the GWP, the picture changes and now the lowest value can be observed for case 1. The normalized GWP of case 1 is −1.5 kg CO_2/kg MeOH, very close to the 1.75 maximum value predicted by the TEA. However, for case 2 the GWP is still slightly higher than in the particular case of MeOH from natural gas, making this process no sense from both an environmental and economic point of view. These results are in line with recent TEA/LCA work that report similar CO_2 abatement numbers and the importance of the energy mixt to the overall process [55–57].

Lastly, we have also evaluated a third scenario where the impact of the cement plant normal operation is considered, being the energy of the MeOH plant still provided by renewable energy sources. While the selection of the source of CO_2 will largely impact the results (i.e., from a cement plant to direct air capture), it is also paramount to assess the total impact of the overall process. The results of this new scenario can be found in Table S9 of the Supplementary Material. A direct comparison between the 2 scenarios is also depicted in Fig. S14. We can observe that, by including the cement plant in the analysis and as expected, most of the indicators deteriorate. The deterioration of the respiratory inorganics (RI), photochemical ozone formation (POF) and acidification potential (AC) indicators is especially severe. Similarly, the normalized GWP increases from the −1.5 kg CO_2/kg MeOH of case 1 to 1.2 kg CO_2/kg MeOH (Case 3 in Fig. 6), implying that the MeOH

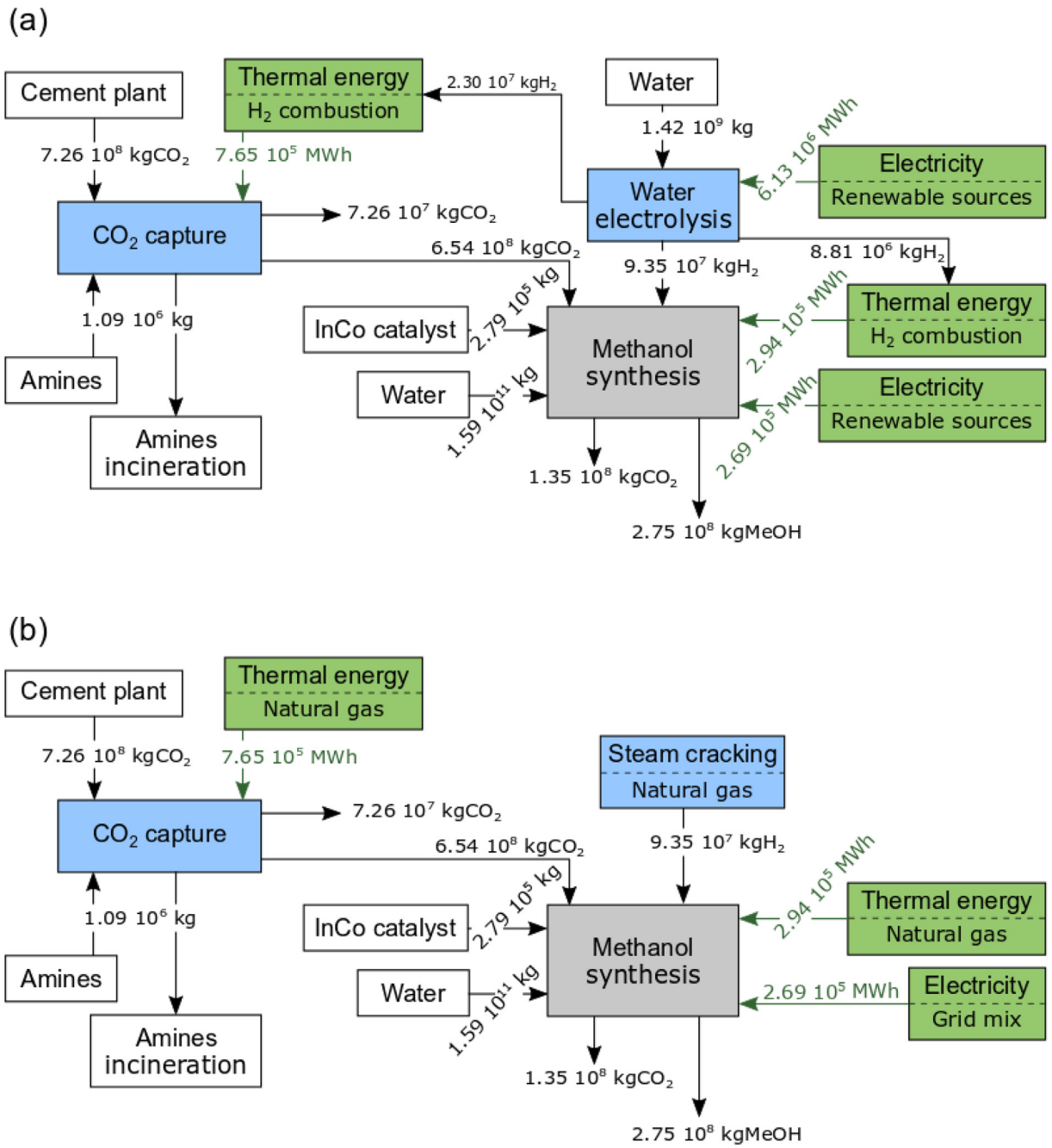

Fig 4. Flow chart for the study cases (a) 1 and (b) 2. The impact of the operation of cement production plant is not considered on the LCA boundaries for these 2 cases.

plant cannot fully offset the emissions of the highly contaminating cement plant.

4. Conclusions

A multidisciplinary study of a methanol production plant from CO_2 has been carried out, assessing from the possibilities of a novel catalyst to the economic viability and the main operational issues coupled with a life cycle assessment. Using a catalyst and a kinetic model made in-house, we have analyzed some relevant parameters for the implementation of the plant from the process and economic point of views, such as CH_4 trace formation, purity, and costs of raw gases, O_2 tolerance in the system, or influence of energy sources.

From experimental results at laboratory scale, an intrinsic kinetic model for the valorization of CO_2 into methanol has been developed using packed bed reactors and an InCo catalyst, which has been demonstrated to be highly active and selective. A comparison of the experimental and calculated data indicated an accurate prediction of the catalytic system by the intrinsic kinetic model and demonstrated that considering the CH_4 formation rate is essential for a truly accurate model.

The implementation of the above kinetic model in the process simulation allowed us to develop a realistic methanol production plant using Aspen Plus® software, taking not only the catalyst CH_4 formation into account but also the important H_2 and CO_2 compression steps.

Based on our results, a successful scale-up of the process will depend on non-catalytic variables, mainly the reactant prices with

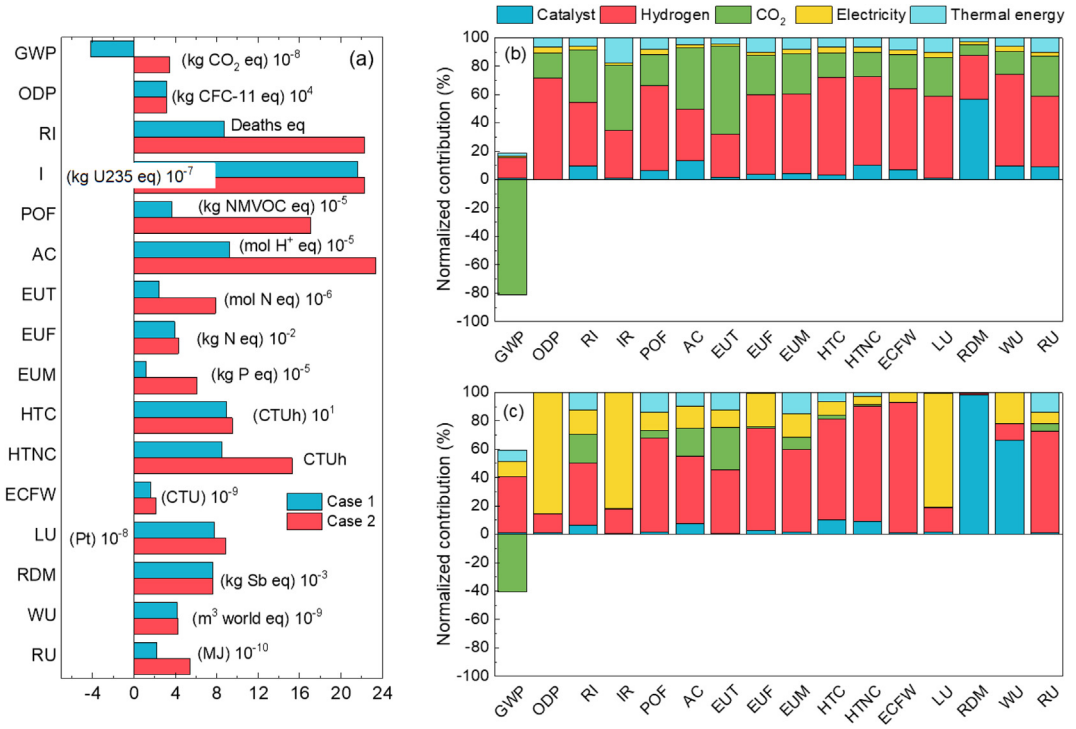

Fig 5. (a) Comparison of the total environmental impact between study cases 1 and 2; comparison of the environmental impacts, distributed by each operation variable, caused by using (b) renewable (case 1) vs. (c) non-renewable sources (case 2).

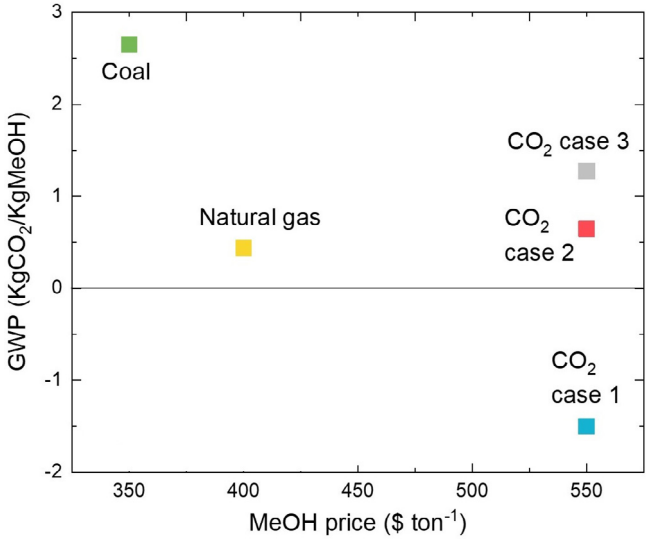

Fig 6. Normalized GWP ($kgCO_2/kgMeOH$) vs. MeOH price ($ ton^{-1}) for different technologies. Case 1 corresponds to MeOH from CO_2 using only renewable energy sources. Case 2 uses traditional energy sources. Case 3 corresponds to case 1 plus the impact of the cement plant. MeOH from coal and natural gas was obtained using data from [53,54].

H_2 itself accounting for most of the final MeOH costs. Our sensitivity analysis confirms that the viability of the plant will largely depend on the fluctuation of H_2 and CO_2 prices, requiring H_2 prices lower than 1.5 $ kg^{-1} or a taxation of CO_2 of at least 300 $ ton^{-1} to reach breakeven.

Nevertheless, our TEA suggests that developing a catalyst that does not produce CH_4 or can withstand large oxygen impurities could have the greatest impact in the process. In particular, the absence of CH_4 could boost the productivity by minimizing the purges, whereas the increase in oxygen tolerance would allow low-cost feed gases to be used in the process, boosting the profitability of the system. Consequently, catalyst development in this particular direction, paying special attention to the CH_4 formation rate and the oxygen tolerance, could affect the viability of the plant more than the current trend of developing more and more active catalyst.

The evaluation of the plant energy sources indicates that, if only renewable energy sources are used and all the indirect sources of CO_2 are obviated, the maximum CO_2 abated in the plant will jump to 1.75 tons per ton of methanol, a 225% increase versus using traditional energy sources. The LCA supports this conclusion with 10 of the 16 indicators studied being lower for the case where only renewable energy is used to run the plan, with especial emphasis to the GWP indicator.

Hence, from an environmental point of view, our results suggest that it does not make sense to produce MeOH from CO_2 if all the energy requirements are also not renewable. Finally, when taking into account the impact of the CO_2 source (a cement plant in our case), most of the LCA indicators are deteriorated and the MeOH plant cannot fully offset the vast emissions of the cement plant. These results highlight the importance of looking at the overall picture when developing a catalyst/process for CO_2 conversion to methanol and, we hope that they help to pave the route for a truly carbon neutral economy.

Declaration of Competing Interest

The authors declare that they have no known competing financial interests or personal relationships that could have appeared to influence the work reported in this paper.

Acknowledgments

The authors gratefully acknowledge financial support from the King Abdullah University of Science and Technology (KAUST). T.

Cordero-Lanzac and A.T. Aguayo acknowledge the financial support received from the Spanish Ministry of Science and Innovation with some ERDF funds (CTQ2016-77812-R) and the Basque Government (IT1218-19). T. Cordero-Lanzac also acknowledges the Spanish Ministry of Education, Culture and Sport for the award of his FPU grant (FPU15-01666). A. Navajas and L.M. Gandía gratefully acknowledge the financial support from Spanish Ministerio de Ciencia, Innovación y Universidades, and the European Regional Development Fund (ERDF/FEDER) (grant RTI2018-096294-B-C31). L.M. Gandía also thanks Banco de Santander and Universidad Pública de Navarra for their financial support under "Programa de Intensificación de la Investigación 2018" initiative.

Appendix A. Supplementary data

Supplementary data to this article can be found online at https://doi.org/10.1016/j.jechem.2021.09.045.

References

[1] G. Leonzio, J. CO2 Util. 27 (2018) 326–354.
[2] A. Rafiee, K. Rajab Khalilpour, D. Milani, M. Panahi, J. Environ, Chem. Eng. 6 (2018) 5771–5794.
[3] A. Álvarez, A. Bansode, A. Urakawa, A.V. Bavykina, T.A. Wezendonk, M. Makkee, J. Gascon, F. Kapteijn, Chem. Rev. 117 (2017) 9804–9838.
[4] N. Mac Dowell, P.S. Fennell, N. Shah, G.C. Maitland, Nat. Clim. Chang. 7 (2017) 243–249.
[5] P. Tian, Y. Wei, M. Ye, Z. Liu, ACS Catal. 5 (2015) 1922–1938.
[6] S. Zhong, X. Yang, Z. Cao, X. Dong, S.M. Kozlov, L. Falivene, J.K. Huang, X. Zhou, M.N. Hedhili, Z. Lai, K.W. Huang, Y. Han, L. Cavallo, L.J. Li, Chem. Commun. 54 (2018) 11324–11327.
[7] L. Wang, M. Ghoussoub, H. Wang, Y. Shao, W. Sun, A.A. Tountas, T.E. Wood, H. Li, J.Y.Y. Loh, Y. Dong, M. Xia, Y. Li, S. Wang, J. Jia, C. Qiu, C. Qian, N.P. Kherani, L. He, X. Zhang, G.A. Ozin, Joule 2 (2018) 1369–1381.
[8] S. Brynolf, M. Taljegard, M. Grahn, J. Hansson, Renew. Sustain. Energy Rev. 81 (2018) 1887–1905.
[9] G. Zang, P. Sun, A. Elgowainy, A. Bafana, M. Wang, Environ. Sci. Technol. 55 (2021) 3888–3897.
[10] J. Wang, G. Li, Z. Li, C. Tang, Z. Feng, H. An, H. Liu, T. Liu, C. Li, Sci. Adv. 3 (2017) 1701290.
[11] E.S. Gutterød, A. Lazzarini, T. Fjermestad, G. Kaur, M. Manzoli, S. Bordiga, S. Svelle, K.P. Lillerud, E. Skúlason, S. Øien-Ødegaard, A. Nova, U. Olsbye, J. Am. Chem. Soc. 142 (2020) 999–1009.
[12] M.S. Frei, C. Mondelli, A. Cesarini, F. Krumeich, R. Hauert, J.A. Stewart, D. Curulla Ferré, J. Pérez-Ramírez, ACS Catal. 10 (2020) 1133–1145.
[13] A. Tsoukalou, P.M. Abdala, A. Armutlulu, E. Willinger, A. Fedorov, C.R. Müller, ACS Catal. 10 (2020) 10060–10067.
[14] A. Bavykina, I. Yarulina, A.J. Al Abdulghani, L. Gevers, M.N. Hedhili, X. Miao, A.R. Galilea, A. Pustovarenko, A. Dikhtiarenko, A. Cadiau, A. Aguilar-Tapia, J.L. Hazemann, S.M. Kozlov, S. Oud-Chikh, L. Cavallo, J. Gascon, ACS Catal 9 (2019) 6910–6918.
[15] K.M. Vanden Bussche, G.F. Froment, J. Catal. 161 (1996) 1–10.
[16] C. Seidel, A. Jörke, B. Vollbrecht, A. Seidel-Morgenstern, A. Kienle, Chem. Eng. Sci. 175 (2018) 130–138.
[17] R. Peláez, P. Marín, S. Ordóñez, Fuel Process. Technol. 168 (2017) 40–49.
[18] K. Ahmad, S. Upadhyayula, Int. J. Hydrogen Energy 45 (2020) 1140–1150.
[19] F. Nestler, A.R. Schütze, M. Ouda, M.J. Hadrich, A. Schaadt, S. Bajohr, T. Kolb, Chem. Eng. J. 394 (2020) 124881.
[20] A. Ateka, M. Sánchez-Contador, A. Portillo, J. Bilbao, A.T. Aguayo, Fuel Process. Technol. 206 (2020) 106434.
[21] É.S. Van-Dal, C. Bouallou, J. Clean. Prod. 57 (2013) 38–45.
[22] D. Milani, R. Khalilpour, G. Zahedi, A. Abbas, J. CO2 Util. 10 (2015) 12–22.
[23] M. Pérez-Fortes, J.C. Schöneberger, A. Boulamanti, E. Tzimas, Appl. Energy 161 (2016) 718–732.
[24] C. Zhang, K.W. Jun, R. Gao, G. Kwak, H.G. Park, Top. Catal. 61 (2018) 1794–1809.
[25] H.S. Fogler, Elements of Chemical Reaction Engineering, 3rd ed., Prentice-Hall, London, 1999.
[26] T. Cordero-Lanzac, A.T. Aguayo, A.G. Gayubo, P. Castaño, J. Bilbao, Chem. Eng. J. 331 (2018) 818–830.
[27] A.T. Aguayo, J. Ereña, D. Mier, J.M.J.M. Arandes, M. Olazar, J. Bilbao, Ind. Eng. Chem. Res. 46 (2007) 5522–5530.
[28] S. Szima, C.C. Cormos, J. CO2 Util. 24 (2018) 555–563.
[29] Commission of Experts. Spanish Government, Analisis y Propuestas Para La, Descarbonización, Madrid, 2018, pp. 1–546.
[30] REData - Generación Red Eléctrica de España, 2021. https://www.ree.es/en/datos/generation.
[31] J. Li, H. Huang, N. Kobayashi, Energy Procedia 142 (2017) 1083–1088.
[32] S. Fazio, F. Biganzioli, V. De Laurentiis, L. Zampori, S. Sala, E. Diaconu, Supporting Information to the Characterisation Factors of Recommended EF Life Cycle Impact Assessment Methods (Version 2, from ILCD to EF 3.0), Publications Office of the European Union, Luxembourg, 2018, pp. 1–42.
[33] A. Ramirez, P. Ticali, D. Salusso, T. Cordero-Lanzac, S. Ould-Chikh, C. Ahoba-Sam, A.L. Bugaev, E. Borfecchia, S. Morandi, M. Signorile, S. Bordiga, J. Gascon, U. Olsbye, JACS Au (2021), https://doi.org/10.1021/jacsau.1c00302.
[34] J. Ereña, I. Sierra, A.T. Aguayo, A. Ateka, M. Olazar, J. Bilbao, Chem. Eng. J. 174 (2011) 660–667.
[35] J. Ott, V. Gronemann, F. Pontzen, E. Fielder, G. Grossmann, D.B. Kersebohm, G. Weiss, C. Witte, Methanol, Wiley-VCH Verlag GmbH & Co. KGaA, Weinheim, 2012.
[36] S. Ong, C. Campbell, P. Denholm, R. Margolis, G. Heath, Land-Use Requirements for Solar Power Plants in the United States, National Renewable Energy Laboratory (U.S, Golden, 2013, pp. 1–47.
[37] P. Ruiz, W. Nijs, D. Tarvydas, A. Sgobbi, A. Zucker, R. Pilli, R. Jonsson, A. Camia, C. Thiel, C. Hoyer-Klick, F. Dalla Longa, T. Kober, J. Badger, P. Volker, B.S. Elbersen, A. Brosowski, D. Thrän, Energy Strateg. Rev. 26 (2019) 100379.
[38] K. Eurek, P. Sullivan, M. Gleason, D. Hettinger, D. Heimiller, A. Lopez, Energy Econ. 64 (2017) 552–567.
[39] BloombergNEF, New Energy Outlook 2019, n.d. https://about.bnef.com/new-energy-outlook/
[40] M. Yekini Suberu, M. Wazir Mustafa, N. Bashir, Renew. Sustain. Energy Rev. 35 (2014) 499–514.
[41] C. Chen, A. Yang, Energy Convers. Manag. 228 (2021) 113673.
[42] G. Dolan, Methanol: Renewable Hydrogen Carrier Fuel, Methanol Institute CaFCP Working Group Meeting, Washington D.C, 2019, pp. 1–45.
[43] C. Bergins, E.L. Fox, K.C. Tran, P. Wuebben, ATZextra Worldw. 21 (2016) 22–25.
[44] H. Dagdougui, R. Sacile, C. Bersani, A. Ouammi, Hydrogen Infrastructure for Energy Applications, Elsevier Inc.,Netherlands, 2018, pp. 7–21.
[45] J. Yates, R. Daiyan, R. Patterson, R. Egan, R. Amal, A. Ho-Baille, N.L. Chang, Cell Reports Phys. Sci. 1 (2020) 100209.
[46] R.T.J. Porter, M. Fairweather, C. Kolster, N. Mac Dowell, N. Shah, R.M. Woolley, Int. J. Greenh. Gas Control 57 (2017) 185–195.
[47] CLARIANT Catalysts for Methanol Synthesis, Product Data Sheet, 2017. https://www.clariant.com/en/Solutions/Products/2019/02/14/13/39/MegaMax-800.
[48] Z. Abbas, T. Mezher, M.R.M. Abu-Zahr, Energy Procedia 37 (2013) 2389–2396.
[49] T. Wiesmann, C. Hamel, S. Kaluza, Chemie-Ingenieur-Technik 90 (2018) 1446–1452.
[50] BASF, 0.1% Pd/AS R5279, Product Data Sheet, 2015. https://catalysts.basf.com/products/0-1-pd-as-r-5279
[51] Y. Ligen, H. Vrubel, H. Girault, Int. J. Hydrogen Energy 45 (2020) 10639–10647.
[52] G. Saur, Wind-To-Hydrogen Project: Electrolyzer Capital Cost Study, National Renewable Energy Laboratory (U.S.), (2008) 1–48.
[53] R. Kajaste, M. Hurme, P. Oinas, AIMS Energy 6 (2018) 1074–1102.
[54] G. Harp, K.C. Tran, C. Bergins, T. Buddenberg, I. Drach, O. Sigurbjornsson, Application of Power to Methanol Technology to Integrated Steelworks for Profitability, Conversion Efficiency, and CO2 Reduction, 2nd European Steel Technology and Application, Duesseldorf, 2015.
[55] J. Nyári, M. Magdeldin, M. Larmi, M. Järvinen, A. Santasalo-Aarnio, J. CO2 Util. 39 (2020) 101166.
[56] C. Chen, Y. Lu, R. Banares-Alcantara, Appl. Energy 243 (2019) 71–90.
[57] A. González-Garay, M.S. Frei, A. Al-Qahtani, C. Mondelli, G. Guillén-Gosálbez, J. Pérez-Ramírez, Energy Environ. Sci. 12 (2019) 3425–3436.